Plant Science 196 (2012) 107–116

Contents lists available at SciVerse ScienceDirect

Plant Science

journal homepage: www.elsevier.com/locate/plantsci

# The chlorotic symptom induced by *Sunflower chlorotic mottle virus* is associated with changes in redox-related gene expression and metabolites☆

Marianela Rodríguez[a,**], Nacira Muñoz[a,c], Sergio Lenardon[b], Ramiro Lascano[a,c,*]

[a] *Instituto de Fisiología y Recursos Genéticos Vegetales (IFRGV), Centro de Investigaciones Agropecuarias (CIAP), Instituto Nacional de Tecnología Agropecuaria (INTA), Camino a 60 Cuadras Km 5 ½, X5020 ICA, Córdoba, Argentina*

[b] *Instituto de Patología Vegetal (IPAVE), Centro de Investigaciones Agropecuarias (CIAP), Instituto Nacional de Tecnología Agropecuaria (INTA), Camino a 60 Cuadras Km 5 ½, X5020 ICA, Córdoba, Argentina*

[c] *Cátedra de Fisiología Vegetal, FCEFyN, Universidad Nacional de Córdoba, Argentina*

ARTICLE INFO

*Article history:*
Received 13 February 2012
Received in revised form 10 August 2012
Accepted 11 August 2012
Available online 18 August 2012

*Keywords:*
Gene expression
Redox state
Symptom development
SuCMoV
Sunflower

ABSTRACT

Systemic infections are commonly associated with changes in host metabolism and gene expression. *Sunflower chlorotic mottle virus* (SuCMoV) causes systemic infection with sugar increase, photoinhibition and increase in antioxidant enzyme activities before chlorotic symptom appearance in sunflower leaves. The aim of this study was to determine if chlorotic symptom development induced by SuCMoV infection is accompanied by changes in different redox-related metabolites and transcripts. Symptom development was analyzed in the second pair of leaves (systemic infection) at different post-inoculation times: before symptom appearance (BS, 4 dpi), and at an early (ES, 7 dpi) and later stage (LS, 12 dpi) of symptom expression. The results showed that the virus reaches the second pair of leaves at 4 dpi. A positive correlation between chlorotic symptom and number of viral copies was also observed. Changes in hydrogen peroxide, glutathione, pyridine nucleotides and ATP content were observed since symptom appearance (ES, 7 dpi). The expression of some of the genes analyzed was also strongly affected by SuCMoV infection. Specifically, down-regulation of both chloroplast-encoded genes and chloroplast-targeted genes: *psbA*, *rbcS*, *Cu/Zn sod*, *Fe sod*, *phosphoglycolate phosphatase*, *psbO*, *psaH* and *fnr* was present, whereas the expression of cytoplasmic-targeted genes, *apx1*, and *Cu/Zn sod* was up-regulated. Mitochondrial *Mn sod* decreased at BS stage and *aox* decreased only at ES stage. Peroxisomal catalase (*cat-2*) was lower at BS and LS stages. All these results suggest that SuCMoV infection induces progressive changes in determinants of redox homeostasis associated with chlorotic symptom development.



*Abbreviations:* AOX, alternative oxidase; APX, ascorbate peroxidase; BS, before symptom expression; CAT, catalase; cp29, chloroplast pigment-binding protein; DEPC, diethylpyrocarbonate; DGC, Di Riezo, Guzmán and Casanoves statistical test in Infostat; DTNB, 5,5′-dithio-bis (2-nitrobenzoic acid); DTT, dithiothreitol; ES, early symptom expression; EDTA, ethylenediaminotetraacetic acid; fnr, Electron carrier (ox/red) ferredoxin reductase; FW, fresh weight; GO, glycolate oxidase; GR, glutathione reductase; GSH, reduced glutathione; GSSG, oxidate glutathione; LS, late symptom expression; NAD(P), total pyridine nucleotide; OEC, oxygen evolving complex; PEG, polyethylenglycol; psaH, photosystem I subunit H-2; psbA, D1 protein component of the PSII reaction center; psbO, 33 kDa extrinsic proteins of the photosystem II oxygen evolving complex; PVPP, polyvinylpolypyrrolidone; rbcS, ribulose 1,5 bisphosphate carboxylase oxygenase small subunit; ROS, reactive oxygen species; SDS, sodium dodecyl sulfate; SOD, superoxide dismutase; SuCMoV, *Sunflower chlorotic mottle virus*; TCA, trichloroacetic acid.

☆ In this manuscript, NAD(P) is used for total pools of reduced and oxidized forms or where the distinction between the two forms is unnecessary. $NAD(P)^+$ is used to make specific reference to the oxidized forms.

* Corresponding author at: Instituto de Fisiología y Recursos Genéticos Vegetales (IFRGV), Centro de Investigaciones Agropecuarias (CIAP), Instituto Nacional de Tecnología Agropecuaria (INTA), Camino a 60 Cuadras Km 5 ½, X5020 ICA, Córdoba, Argentina. Tel.: +54 351 4974343; fax: +54 351 4974330.

** Corresponding author.

*E-mail addresses:* zmarianela@hotmail.com (M. Rodríguez), hrlascano@correo.inta.gov.ar (R. Lascano).

0168-9452/$ – see front matter © 2012 Elsevier Ireland Ltd. All rights reserved.
http://dx.doi.org/10.1016/j.plantsci.2012.08.008

## 1. Introduction

*Sunflower chlorotic mottle virus* (SuCMoV) is a member of the genus Potyvirus; it is located in the cell cytoplasm and causes systemic infections in sunflower plants, leading to chlorotic mottling and severe growth reductions and yield losses [1]. Systemic infection in plants relies on complex molecular interactions between the invading virus and the host plant [2,3]. Accumulation of viral proteins is commonly associated with some consequences for host gene expression and metabolism as well as alterations in plant growth and development; all of those consequences are important components of symptom development [3].

In a previous report we showed that chlorotic symptom development during compatible sunflower–SuCMoV interaction was correlated with early sugar increases and these increases significantly reduced quantum efficiency of PSII photochemistry (photoinhibition) and photosynthesis related protein levels (D1 and RubisCO), reduced apoplastic ROS production and increased antioxidant enzyme activities (SOD; APX; GR) [4]. Chloroplasts are generally the plant cell organelles most sensitive to viral infection and one of the cellular compartments in which the down-regulated genes are over-repressed during compatible plant–virus interaction [5]. All these responses, which are related to photoinhibion, chlorosis and redox changes, are characteristic of natural senescence process [6,7].

Viral infection induces modification in electron transport as a result of an impaired photosynthetic and respiratory activity, and may generate reactive oxygen species (ROS), such as singlet oxygen ($^1O_2$), superoxide radical ($O_2^{\bullet -}$), hydrogen peroxide ($H_2O_2$), and hydroxyl radical ($OH^{\bullet}$) [8]. Chloroplasts, mitochondria and peroxisomes are the main sources of ROS in plants [9]. In addition, the NADPH oxidase complex is a major source of apoplastic ROS [10]. The NADPH oxidase complex is responsible for early ROS generation in plant–pathogen interactions and exhibits monophasic or biphasic patterns in compatible and incompatible interactions, respectively [11]. Arias et al. [12] demonstrated that the sunflower–SuCMoV compatible interaction has a monophasic pattern response of apoplastic ROS generation. Subsequent work of our group indicated that NADPH oxidase activity decreased over the course of infection [4]. Likewise, SuCMoV infection induced antioxidant enzyme activity; this activity was suggested to stop signals generated by ROS increments, which may be involved in triggering defense reactions that otherwise would have contributed to prevent the systemic spread of the virus [12]. Distinct responses of antioxidant system in compatible plant–virus interactions have been reported [12–14]. The defense system in various subcellular compartments forms an integrated network with extensive crosstalk that could be triggered by ROS [15]. The dual role of ROS, as toxic or signaling molecules, is determined by the rates and subcellular location of ROS generation and degradation [15]. The increasingly refined identification of marker transcripts induced by different ROS provides useful tools for distinguishing the operations of different ROS signaling pathways under various stress conditions [16].

Growing evidence suggests a model for redox homeostasis in which the ROS–antioxidant interaction acts as a metabolic interface for signals derived from metabolism and the environment. This interface modulates the appropriate induction of acclimation processes or, alternatively, the execution of cell death programs [17]. Together with ROS, ascorbate, glutathione, sugars, ATP and pyridine nucleotide (NAD(P)) are major determinants of the intracellular redox state, which influence gene expression associated with biotic and abiotic stress responses to maximize defense [18–20]. In addition, recent findings indicate that pathogen-induced changes in the cellular redox environment are sensed by reactive cysteine residues of key regulatory proteins [21]. Moreover, the importance of the endogenous plant glutathione has been increasingly recognized in plant–pathogen interactions due to its contribution to various signaling and defense mechanisms [22 and references therein]. Likewise, pyridine nucleotides are also key players in signaling through ROS since they are crucial in the regulation of both ROS-producing and ROS-scavenging systems in plants [15,18,19].

There is limited information on the physiological and molecular changes induced during compatible sunflower–SuCMoV interaction. Our previous characterization showed early sugar increases and photoinhibition induced by SuCMoV infection. Considering the theoretical context mentioned, we hypothesized that early responses of sugar increases and photoinhibition induced by SuCMoV infection would provoke changes in different redox-related metabolites and gene expression, which are associated with chlorotic symptom development.

The aim of this study was to assess changes in key redox determinants, such as hydrogen peroxide, ascorbate, glutathione and pyridine nucleotides, together with the expression of genes related to photosynthetic, respiratory and antioxidant systems, in the three-stage kinetics of infection during chlorotic symptom development.

## 2. Material and methods

### 2.1. Plant material

Sunflower (*Helianthus annuus* L.) line L2 seeds were provided by Advanta Semillas SAIC, Balcarce, Argentina. Seeds were sown in pots with sterile soil and cultivated in a growth chamber under controlled 250 μmol photons $m^{-2}$ $s^{-1}$ light with 16 h photoperiod at 25 °C and 65% humidity. The common strain of SuCMoV [23] was maintained in *Nicotiana occidentalis* L. and symptomatic leaves were freeze-dried and kept at −20 °C. Sunflower plants at the vegetative stages V1–V2 [24] were rub-inoculated on the upper surfaces of the first pair of leaves with an infected leaf homogenate (1:5 w/v in 0.05M $Na_2HPO_4$, pH 7.5) using 600-mesh carborundum as abrasive. Control plants were mock-inoculated with buffer and abrasive. To evaluate systemically infected leaves, samples were always taken from the second pair of leaves 4 days post-inoculation (dpi) (before symptom expression, BS), 7 dpi (early symptom expression, ES), and 12 dpi (late symptom expression, LS).

### 2.2. Total chlorophyll content

The amount of chlorophyll in leaves was estimated using a handheld SPAD CL01 meter (Hansatech Instruments, Pentney King's Lynn, UK). This provides a unitless index ranging from 0 to 100 that is proportional to leaf chlorophyll content [25]. The second pair of leaves was divided into three parts (base, middle and tip). Average SPAD readings were calculated from four measurements.

### 2.3. SuCMoV accumulation

A real-time quantitative RT-PCR assay, based on SYBR Green [26], was developed to detect and quantify SuCMoV.

A specific SuCMoV nucleotide sequence (132 bp) of the capsid protein (CP) gene amplified by RT-PCR, consisting of the target region for the real-time primers, was inserted into TOPO-TA 2.1 (Invitrogen, Carlsbad, CA) and cloned into *Escherichia coli* DH5α. Transformants were selected by ampicillin resistance. The plasmid was purified and used as target for standard curves. Conversion of microgram of single stranded DNA to picomole was performed considering the average molecular weight of a ribonucleotide (340 Da) and the number of bases of the transcript

(Nb). The following mathematical formula was applied: pmol of ssDNA = mg (of ssDNA) × ($10^6$ pg/mg) × (1 pmol/340 pg) × (1/Nb). Avogadro constant (Avogadro, 1811) was used to estimate the number of transcripts ($6.023 \times 10^{23}$ molecules/mol). Number of transcripts was calculated per 2 μl, which was the volume used as template in each quantitative real-time RT-PCR. Ten-fold serial dilutions of the transcripts (from $1 \times 10^6$ to $1 \times 10^3$) were employed to generate the standard curve.

### 2.4. ATP content

ATP concentration was determined by means of an ENLITEN® ATP Assay System Bioluminescence Detection kit (Promega, Madison, WI, USA). Extraction of ATP: frozen leaf samples (20 mg fresh weight) were ground to a fine powder with liquid nitrogen and homogenized, suspended in 0.2 ml of 2.5% trichloracetic acid (TCA). Samples were centrifuged at 18,000 × *g* at 4 °C for 15 min. The samples were diluted 40 times with 0.1 M Tris acetate buffer (pH 7.75) before assessment.

To quantify ATP, 50 μl of Enliten Luciferase/Luciferin (L/L) medium (rL/L reagent, reconstitution buffer) was added to 10 μl of sample and 90 μl of 0.1 M tris-Acetate buffer (pH 7.75) in the microplate. The luminescence of this reaction was measured with a Turner BioSystems Veritas™ Microplate Luminometer at 25 °C (Promega, Madison, WI, USA). A calibration curve was generated for each luciferase assay by serial dilution of an ATP standard. To check for ATP contamination, we used equal volumes of the component to be tested and the rL/L Reagent.

### 2.5. Hydrogen peroxide

Hydrogen peroxide was estimated in leaf extracts, according to Guilbault et al. [27], including a blank with catalase (EC 1.11.1.6) for each sample. Frozen leaf samples were ground to a fine powder with liquid nitrogen and homogenized 1/10 (w/v) in 50 mM potassium phosphate buffer (pH 7.5), containing 1 mM EDTA and 1% PVPP (polyvinylpolypyrrolidone). Homogenates were centrifuged at 16,000 × *g* at 4 °C for 25 min and the supernatant was used to determine protein and hydrogen peroxide concentrations.

### 2.6. Glutathione and ascorbate content

Leaf samples were prepared for glutathione and ascorbate analyses by homogenizing 100 mg leaf material (fresh weight) in 1 ml of cold 3% TCA and 100 mg PVPP. The homogenate was centrifuged at 10,000 × *g* at 4 °C for 15 min and the supernatant was collected for analyses of glutathione and ascorbate.

Reduced glutathione content was determined spectrophotometrically at 405 nm in acid-soluble extracts, according to Anderson et al. [28] with modifications. The samples were neutralized with potassium 200 mM phosphate buffer pH 7.0 and incubated with 10 mM 5,5′-dithio-bis(2-nitrobenzoic acid) (DTNB) during 15 min. Total glutathione content was determined in neutralized samples after reduction of oxidized glutathione (GSSG) with 1 U of wheat glutathione reductase (Sigma Chemical Co.), 1 mM EDTA, 3 mM $MgCl_2$, and 150 mM NADPH.

Total ascorbate content was determined according to Gillespie and Ainsworth [29] with modifications. The reaction mixture for total ascorbate contained a 50-μl aliquot of the supernatant, 25 μl of 150 mM phosphate buffer (pH 7.4) containing 5 mM EDTA, and 25 μl of 10 mM DTT; samples were incubated at room temperature for 10 min. After that, the mix was incubated with 25 μl of 0.5% N-ethylmaleimide (NEM), 16.6% orthophosphoric acid ($H_3PO_4$), 1.33% α–α′bipyridyl and 50 μl of 0.5% $FeCl_3$ at 37 °C for 60 min. The samples were measured at 525 nm in ELISA MRX II. Reduced ascorbic acid content was determined by the same protocol without addition of NEM and DTT.

### 2.7. Pyridine nucleotides content

Pyridine nucleotides were assayed by spectrophotometric plate reader method, as described by Queval and Noctor [30].

### 2.8. Total protein content

Soluble proteins were estimated according to Bradford [31]. Bovine serum albumin was used as standard for the calibration curves.

### 2.9. RNA extraction

Leaf samples subjected to different treatments were homogenized in cold mortar with trizol (1/10 plant tissue/phenol), mixed for 1 min and incubated at room temperature for 5 min. Then, 0.2 ml chloroform per ml of trizol was added and incubated at room temperature for 3 min. After incubation, the samples were centrifuged at 14,000 rpm at 4 °C for 15 min. The aqueous phase was transferred to clean tubes and 1 volume of isopropanol was added and then incubated at room temperature for 10 min and centrifuged at 14,000 rpm at 4 °C for 15 min. The precipitate was washed with 70% ethanol and centrifuged again at 14,000 rpm at 4 °C for 15 min. The precipitate was dried, resuspended in DEPC water and its concentration was quantified in NanoDrop spectrophotometer ND-1000 (NanoDrop Technologies, Inc.). Purified RNA was treated with DNase I (Invitrogen) to remove any contaminating genomic DNA, according to the manufacturer's instruction.

### 2.10. Analysis of gene expression

Based on cDNA sequences from a sunflower EST catalogue (http://compbio.dfci.harvard.edu/tgi/tgipage.html), specific primers were designed to determine the expression of 15 genes (Supplementary Table 1) by real-time PCR.

### 2.11. qRT-PCR

DNA-free RNA (1–2.5 μg) was used with oligo(dT) for first strand cDNA synthesis using the Moloney murine leukemia virus reverse transcriptase for RT-PCR (Promega), according to the manufacturer's instruction. Primers used for qRT-PCR were designed using AmplifX version 1.5.4 by Nicolas Jullien (http://ifrjr.nord.univ-mrs.fr/AmplifX-Home-page) with the following criteria: melting temperature of 61 °C, PCR amplicon lengths between100 and 220 bp, and yielding primer sequences with lengths of 20 nucleotides and guanine–cytosine contents between 40% and 60%. The list of the primers used in this study is available in Supplementary Table 1. qRT-PCR was performed in thermocycler iQ5 (Bio Rad) with iQ SYBR Green Supermix (Bio Rad), according to the manufacturer's instruction. Values were normalized based on those obtained from *actin* as housekeeping gene. Relative expression levels were calculated by $2^{-\Delta Ct}$ method which is a variation of the Livak and Schmittgen [32] method.

## 3. Results

### 3.1. Symptomatology and viral accumulation

Infected plants usually present individual, brilliant yellow blotches that later coalesce, reducing and distorting leaf morphology and producing plant stunting. In a previous study, we were not able to determine the presence of virus in leaves before the

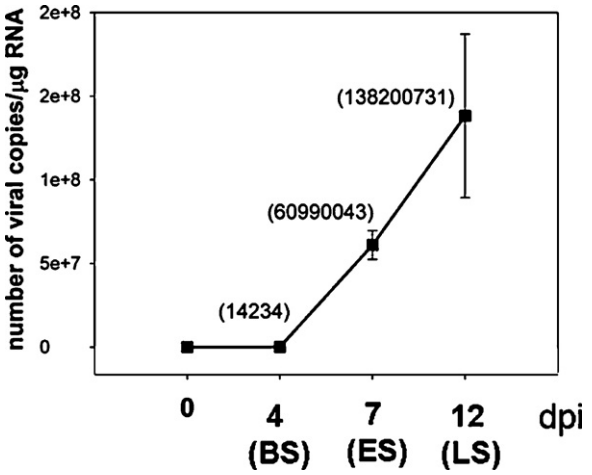


**Fig. 1.** SuCMoV qRT-PCR accumulation analysis (expressed as number of viral copies/µg RNA) in systemic leaves from SuCMoV-inoculated plants at three stages of SuCMoV infection. BS: before symptom expression (4 dpi), ES: early symptom expression (7 dpi), LS: late symptom expression (12 dpi). Absolute values are given in bracket. Results are means from three plants ± SE of three independent experiments.

appearance of chlorotic symptoms using protein immunoblot analysis and end-time PCR in the second pair of leaves (systemically infected leaves) [12]. This could be related to the low sensitivity of the method and low virus concentration. To determine the day on which SuCMoV was present in the second pair of leaves, we used quantitative qRT-PCR analysis. Under our experimental condition, SuCMoV reached the second pair of leaves at 4 dpi (BS stage) (Fig. 1).

Even though we found that in SuCMoV-inoculated plants in the first pair of leaves the virus reached the second pair of leaves at 4 dpi, symptoms did not appear until 7 dpi and total chlorophyll content did not decrease until 12 dpi in this pair of leaves [4]. To further characterize the effects of SuCMoV infection, chlorotic symptom development was evaluated by measuring yellowing in three parts of the systemically infected second pair of leaves (base, middle and tip) with SPAD. The results showed that leaf chlorotic symptom appeared at the leaf base and progressed to the tip. The differences between control and infected plants began to be significant at 7 dpi in the leaf base, at 8 dpi in the middle and at 12 dpi in the tip (Fig. 2). These results clearly show the spatial and temporal development of chlorotic symptom induced by SuCMoV. In addition, symptom development was accompanied by a constant increase of SuCMoV genome copies (Figs. 1 and 2).

### 3.2. Redox-related metabolites: hydrogen peroxide, non-enzymatic antioxidant, pyridine nucleotide and ATP changes during SuCMoV infection

In a previous study we have demonstrated that SuCMoV induces photoinhibition and changes in soluble sugar content, apoplastic ROS and antioxidant system activities, which are determinants of cellular redox state [4]. To further characterize the effects of SuCMoV infection on cellular redox state, the key compounds hydrogen peroxide, ascorbate, glutathione, pyridine nucleotides and ATP were measured.

Hydrogen peroxide content was measured in leaf extracts using 3–5 dinitrosalicylic acid, according to Guilbault et al. [27]. The levels of hydrogen peroxide were significantly increased in SuCMoV-infected leaves at ES and LS stages (Fig. 3). Reduced glutathione was higher in infected leaves than in control; there was no effect on total glutathione content (Fig. 4A). Furthermore, oxidized glutathione was lower in infected leaves (Fig. 4A). Therefore, we observed an increase in couple redox with symptom appearance (Fig. 4B). Interestingly, the analysis of ascorbic acid content in infected leaves

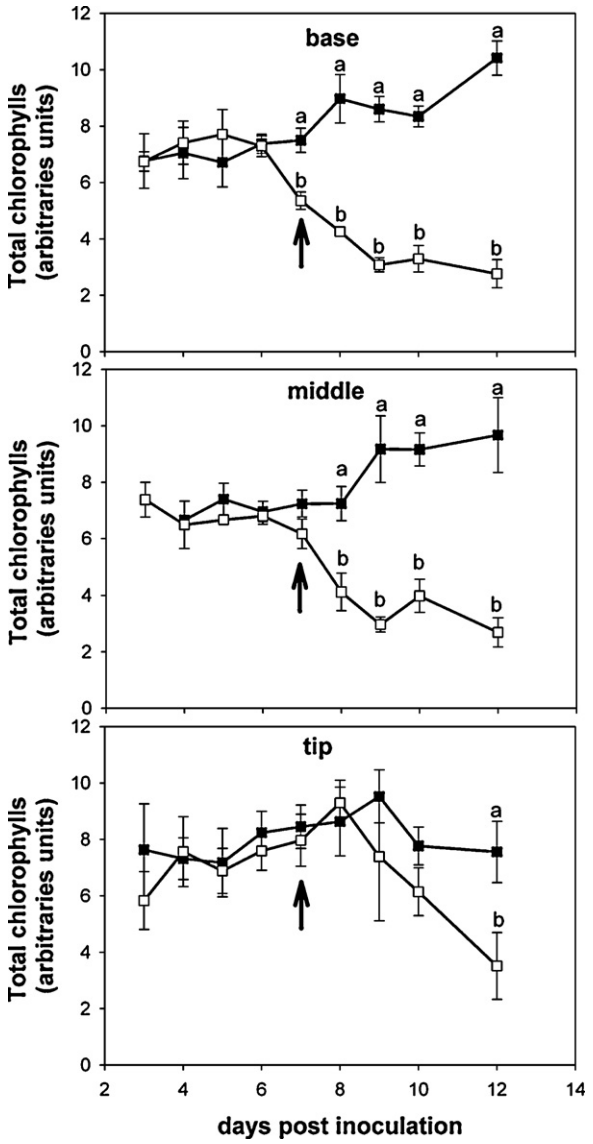


**Fig. 2.** Total chlorophyll content during the course of infection. Total chlorophyll content was estimated in three parts of systemic leaves at the base, middle and tip with SPAD from SuCMoV-inoculated (SuCMoV) and mock-inoculated (Control) plants at different times post SuCMoV inoculation. Symptom appearance is indicated with a black arrow. Results are means from 12 plants ± SE of three independent experiments. Different letters indicate significant differences with controls ($p < 0.05$, DGC).

revealed that no changes occurred during viral infection (data not shown). NADH content was higher in infected leaves than in control since BS stage, whereas $NAD^+$ rose at ES and LS stages (Fig. 5A). In addition, $NADP^+$ and NADPH increased only at LS stage (Fig. 6A). However, pyridine nucleotides did not show any redox alteration (Figs. 5 and 6B). ATP content only increased significantly at LS (Fig. 7) and it was correlated with the maximum viral genome copies obtained (Fig. 1).

### 3.3. Effects of SuCMoV infection on gene expression

Transcripts reduction of several chloroplast-targeted proteins has been observed associated with potyvirus infections [33]. In general, sunflower plants infected with SuCMoV showed a significant decrease in gene expression of *psbO*, *psbA*, *psaH*, *fnr* and *rbcS*, except *cp29*. Likewise, the drop in gene expression levels was dependent on plant–viral stage. The transcript levels of *fnr* and *psaH* decreased

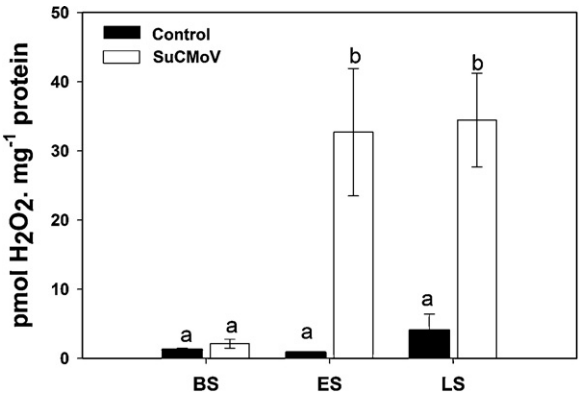


**Fig. 3.** Hydrogen peroxide levels in systemic leaves from SuCMoV-inoculated (SuCMoV) and mock-inoculated (Control) plants at three stages of SuCMoV infection: BS: before symptom expression (4 dpi), ES: early symptom expression (7 dpi), LS: late symptom expression (12 dpi). Results are expressed as means ± SE of 12 plants in three independent experiments. Different letters indicate significant differences with controls ($p < 0.05$, DGC).

at all infection stages, whereas *psbO*, *psbA* and *rbcS* showed significant decreases only at LS stage (Fig. 8).

Fig. 9 shows transcript levels of antioxidant enzymes. At BS stage we observed a significant increase in cytosolic *apx-1* gene expression, whereas mitochondrial *Mn-sod* and peroxisomal *cat* showed a significant decrease. Likewise, during ES stage cytosolic *apx-1* remained significantly high and a chloroplastic *Fe-sod* increased, whereas chloroplastic *Cu/Zn sod* dropped notably. During LS stage cytosolic *apx-1* and *Cu/Zn sod* gene expression increased, whereas the expression levels for all analyzed chloroplast genes decreased.

In addition, transcriptional analysis of enzymes involved in photorespiration showed a marked decrease in *phosphoglycolate phosphatase* since the appearance of symptom, whereas *glycolate oxidase* did not change. On the other hand, *aox-1* transcription showed a decrease only at ES stage.

## 4. Discussion

SuCMoV infection induces small chlorotic spots and yellow blotches on sunflower leaves. According to the present results, the virus reached the second pair of leaves (systemic infection) at 4 dpi, three days before symptoms appearance. We have recently demonstrated that SuCMoV infection increased systemic soluble sugar, photoinhibition, degradation of D1 protein and antioxidant enzyme activities before chlorotic symptom appearance (BS, 4 dpi). All SuCMoV-induced effects were increased at ES (7 dpi) and LS (12 dpi) stages [4,12]. Accordingly, the early redox alteration induced by SuCMoV infection might provoke further changes in

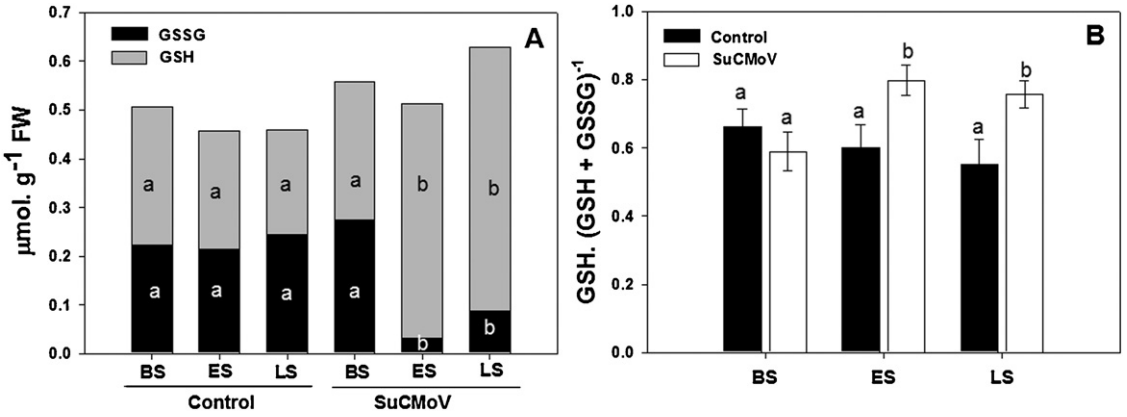


**Fig. 4.** Glutathione content in systemic leaves from SuCMoV-inoculated (SuCMoV) and mock-inoculated (Control) plants at three stages of SuCMoV infection: BS: before symptom expression (4 dpi), ES: early symptom expression (7 dpi), LS: late symptom expression (12 dpi). (A) Reduced glutathione (GSH gray bars) and oxidized glutathione (GSSG black bars). (B) GSH. $(GSH + GSSG)^{-1}$ ratio from SuCMoV-inoculated (SuCMoV white bar) and mock-inoculated (Control black bar) plants. Results are means from 12 plants ± SE of four independent experiments. Different letters indicate significant differences with controls ($p < 0.05$, DGC).

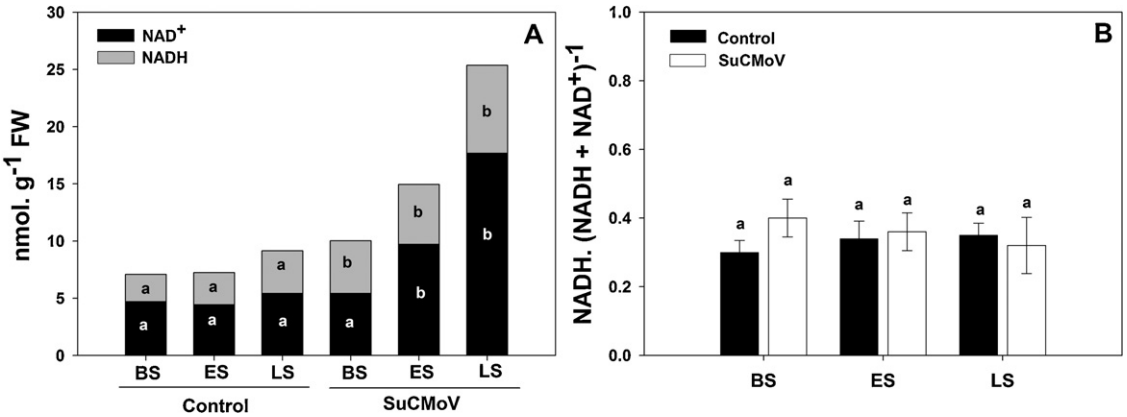


**Fig. 5.** (A) $NAD^+$ and NADH content during SuCMoV infection expressed in nmol $g^{-1}$ FW in systemic leaves from SuCMoV-inoculated (SuCMoV) and mock-inoculated (Control) plants at three stages of SuCMoV infection: BS: before symptom expression (4 dpi), ES: early symptom expression (7 dpi), LS: late symptom expression (12 dpi). $NAD^+$ is shown in black bars and NADH in gray bars. (B) NADH. $(NADH + NAD^+)^{-1}$ ratio from SuCMoV-inoculated (SuCMoV white bar) and mock-inoculated (Control black bar) plants. Results are expressed as means ± SE of 12 plants in three independent experiments. Different letters indicate significant differences with controls ($p < 0.05$, DGC).

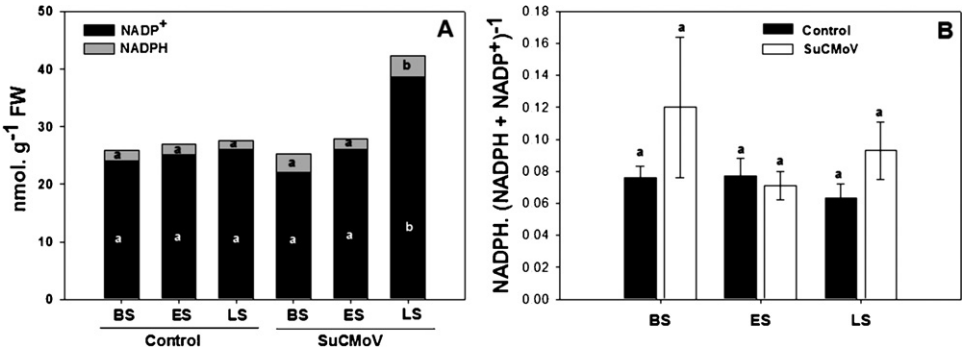


**Fig. 6.** (A) $NADP^+$ and NADPH content during SuCMoV infection expressed in nmol $g^{-1}$ FW in systemic leaves from SuCMoV-inoculated (SuCMoV) and mock-inoculated (Control) plants at three stages of SuCMoV infection: BS: before symptom expression (4 dpi), ES: early symptom expression (7 dpi), LS: late symptom expression (12 dpi). $NADP^+$ is shown in black bars and NADPH in gray bars. (B) NADPH. $(NADPH + NADP^+)^{-1}$ ratio from SuCMoV-inoculated (SuCMoV) (white bar) and mock-inoculated (Control black bar) plants. Results are expressed as means ± SE of 12 plants in three independent experiments. Different letters indicate significant differences with controls ($p < 0.05$, DGC).

different redox-related metabolites and transcripts during chlorotic symptom development.

The major changes of the parameters analyzed were observed since symptom appearance (ES), and remained at LS stage. Noticeably, the absence of significant differences in the redox-related metabolites at BS stage could be related to a low SuCMoV concentration in the leaf. A positive correlation among chlorotic symptom development, redox-related changes and number of viral copies was observed.

Glutathione and ascorbate are the major soluble non-enzymatic ROS scavengers and are important multifunctional metabolites in redox homeostasis, development and defense response [20]. Accordingly, reduced glutathione accumulation, without changes in total glutathione, suggests that there is no de novo synthesis of this compound during SuCMoV infection. The significant increase in glutathione redox couple is supported by a reported increase in glutathione reductase activity [4]. Exogenous reduced glutathione is well known to act in a way similar to pathogen elicitors, activating the expression of defense-related genes, including *PATHOGENESIS-RELATED 1* (*PR1*). Moreover, accumulation of glutathione and changes in its redox state are triggered by pathogen infection [34,35], which could be related to the plant defense induction [21]. Glutathione is mainly located in chloroplasts, and highly reduced glutathione content induces photoinhibition because it increases the degree of quinone A (QA) reduction and consequently decreases electron transport efficiency of PSII [36]. By contrast, $H_2O_2$ treatment increases oxidation of QA and electron transport efficiency of PSII [36]. Previous results indicated that SuCMoV infection induces photoinhibition and degradation of D1 protein at BS stage [4]; the present results indicate an increase in GSH content at ES and LS stages that could be favoring photoinhibitory process. Nevertheless, our results also show an important rise in hydrogen peroxide content in SuCMoV infected leaves. Chloroplasts do not seem to be the main source of intracellular hydrogen peroxide in infected cells (unpublished data). These results are also supported by a previous report indicating that SuCMoV induces SOD, APX and GR activities, which are mainly located in the chloroplasts, and that this phenomenon might be modulating the hydrogen peroxide level in this organelle [4,8]. Likewise, the possibility that an increase in $O_2^1$ might be occurring in the chloroplast between BS and ES stages, which could be involved in the photoinhibition process, cannot be ruled out [37].

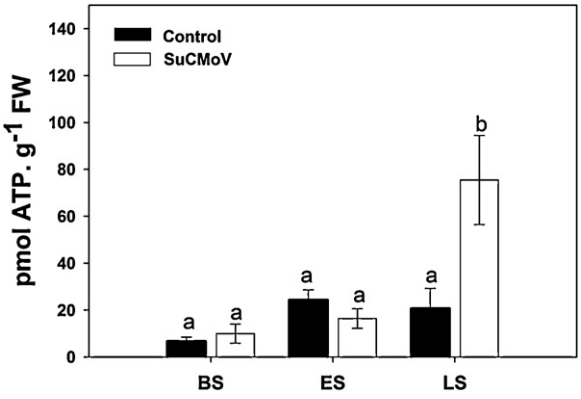


**Fig. 7.** ATP content in systemic leaves from SuCMoV-inoculated (SuCMoV) and mock-inoculated (Control) plants at three stages of SuCMoV infection. BS: before symptom expression (4 dpi), ES: early symptom expression (7 dpi), LS: late symptom expression (12 dpi). Results are means from 4 plants ± SE of four independent experiments. Different letters indicate significant differences with controls ($p < 0.05$, DGC).

Interestingly, ascorbate did not change in any of the three SuCMoV infection stages (data not shown), suggesting the action of a highly efficient ascorbate regeneration system, which network is more complex than mere scavenging within the cellular stress response [17].

The ROS–antioxidant interaction and its subcellular location determine the role of ROS and modulate the expression of the antioxidant system genes [15,38]. In general, our results show that the transcript levels of cytosolic antioxidant enzyme increased during the compatible interaction, whereas the chloroplastic antioxidant enzyme decreased mainly at LS stage. Cytosolic ascorbate peroxidase 1 (*apx-1*) showed enhanced expression since BS stage. Similar responses have been reported in different compatible plant–pathogen interactions [39,40] suggesting a key role for this APX isoform. APX1 expression depends on the redox state of the photosynthetic electron transport chain and the content of glutathione [41,42]. Despite its cytosolic localization, APX1 is required for the protection of chloroplasts against ROS [43]. In addition, cytosolic *Cu/Zn sod* was up-regulated, whereas chloroplastic *Cu/Zn sod* was down-regulated at ES and LS stages.

The peroxisomes are another important intracellular source of hydrogen peroxide [9]. Interestingly, the catalase mRNA down-regulation observed at BS and LS is consistent with enzyme activity observed in a previous report [4] and it might also contribute to an increase in peroxisomal hydrogen peroxide. Transcripts for tobacco CAT1 (equivalent to Arabidopsis CAT2) were found to be strongly down-regulated in a biotic stress [44,45]. Peroxisomal hydrogen peroxide could be also produced by photorespiration pathway. Accordingly, we found that gene expression of *phosphoglycolate phosphatase* decreased at ES and LS stages, whereas gene expression of *glycolate oxidase* did not show any change.

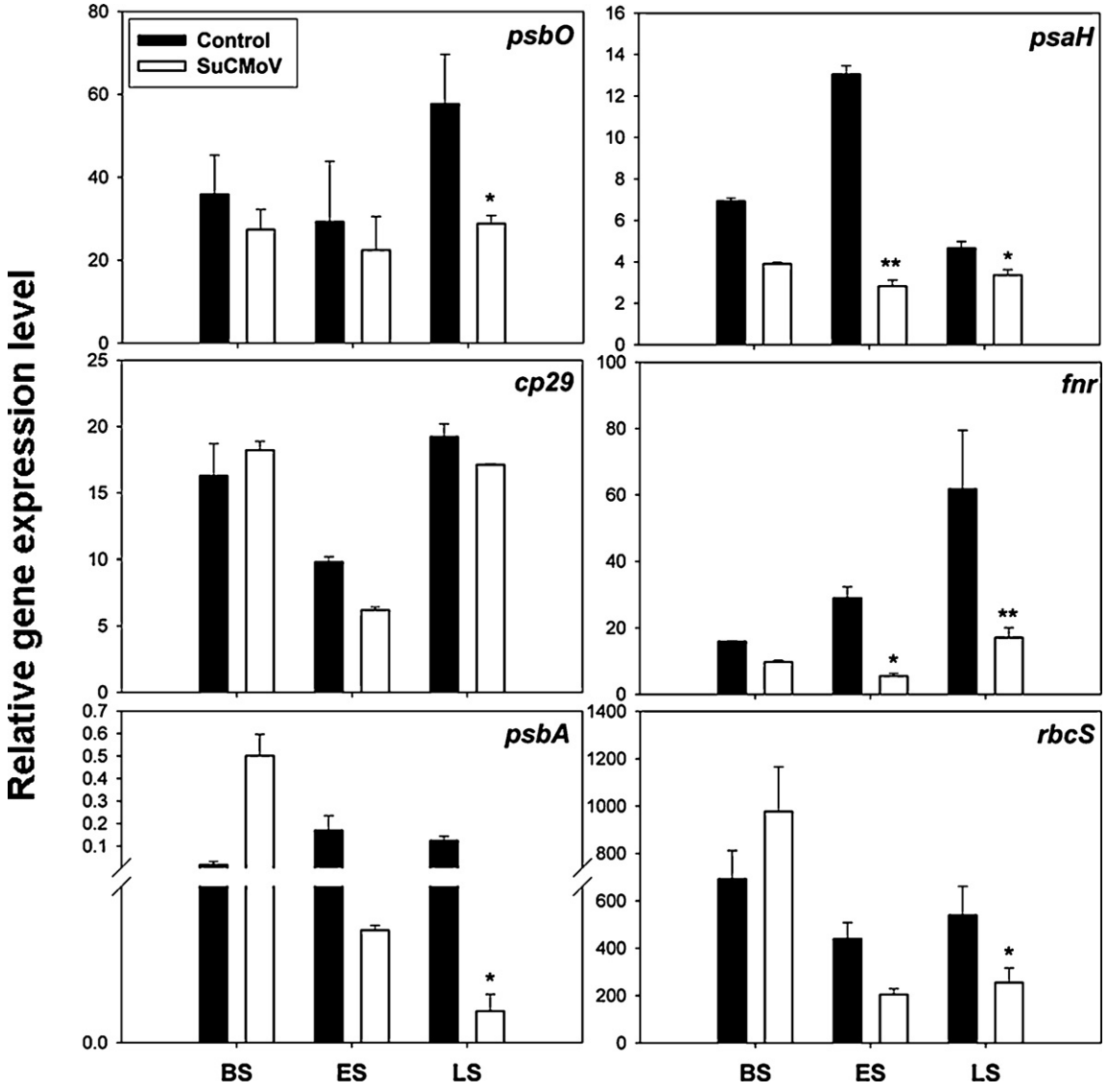


**Fig. 8.** Relative expression of genes related to photosynthesis in systemic leaves from SuCMoV-inoculated (SuCMoV) and mock-inoculated (Control) plants at three stages of SuCMoV infection: BS: before symptom expression (4 dpi), ES: early symptom expression (7 dpi), LS: late symptom expression (12 dpi). Values were normalized based on *ACTIN* as internal reference gene. Means of three independent biological experiments ± SE are shown. Significant differences were calculated by Student's *t*-test, and * and ** indicate significance at the 0.05 and 0.01 levels of confidence, respectively.

The excess of sugar induced by SuCMoV could be associated with increased mitochondrial electron transport, respiratory rates, ROS and ATP generation. Mitochondrial ROS are important players in pathogen symptom development [20]. Alternative oxidase (AOX) activity control mitochondrial superoxide production. The abundance of AOX transcripts, proteins and activity is increased under different stress conditions, including responses to different pathogen attacks [46]. However, our results showed a significant decrease in AOX mRNA level at ES stage during SuCMoV infection. Accordingly, tobacco cells with low AOX produced more ROS and showed up-regulation of antioxidant defenses [47] similar to SuCMoV infection. On the other hand, the ATP content increased at LS stage of SuCMoV infection, at which the respiration is increased and the virus is actively replicated.

Reduction of transcripts of several chloroplast-targeted proteins has been observed associated with potyvirus infections [33]. The present study shows that SuCMoV infection also results in a marked decrease in the expression of some photosynthesis-related genes encoded in both nucleus and chloroplasts.

In particular, a down-regulation of *rbcS* and *psbA* gene expression at LS stage was observed. Transcriptional *rbcS* down-regulation agrees with previous results showing decrease of the RuBisCO protein levels at LS stage [4]. Moreover, there are many studies reporting a clear reduction of *rbcS* transcript accumulation upon pathogen infection [48]. Likewise, a D1 (PsbA) protein decrease since BS stage was demonstrated by our work group [4]; however *psbA* transcript level did not show any change at this early stage. It has been reported that loss of D1 protein during tobacco-TMV (*Tobacco Mosaic Virus*) interaction was not associated with *psbA* mRNA levels [49]. D1 is a protein with a high turnover rate, and its levels in all higher plant chloroplasts depend on transcriptional control, mRNA stability, and principally on the control at the level of initiation and elongation of translation related to thiol redox signaling [50].

Similarly, oxygen evolving complex (OEC) of PSII is one of the main chloroplast targets in viral infection [48,51]; we showed a decrease in *psbO* expression at LS stage. Interestingly, *cp29* expression, a chlorophyll-binding protein of the outer antenna of PSII

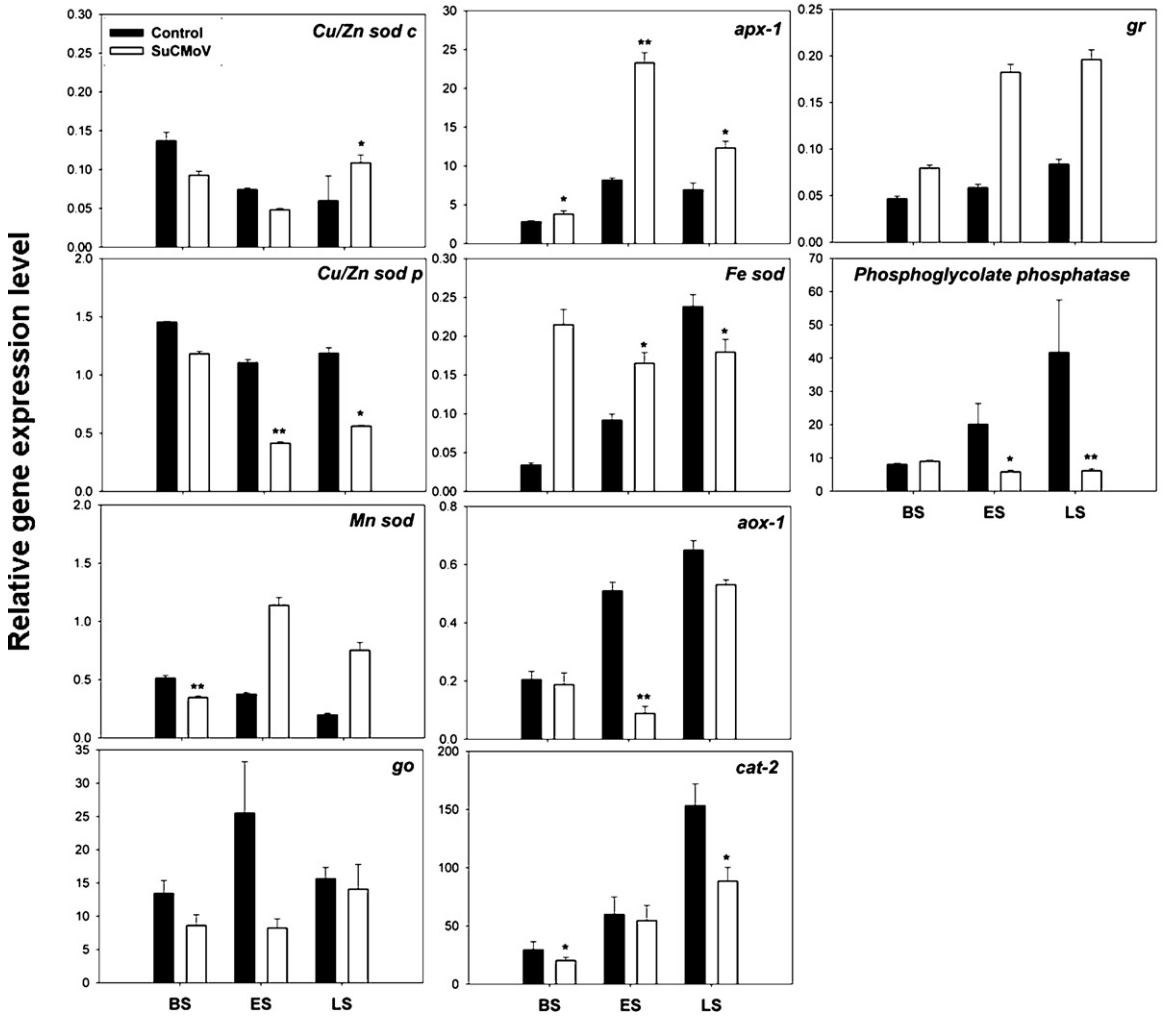


**Fig. 9.** Relative expression of antioxidant system in systemic leaves from SuCMoV-inoculated (SuCMoV) and mock-inoculated (Control) plants at three stages of SuCMoV infection: BS: before symptom expression (4 dpi), ES: early symptom expression (7 dpi), LS: late symptom expression (12 dpi). Values were normalized based on *ACTIN* gene as internal reference. Means of three independent biological experiments ± SE are shown. Significant differences were calculated by Student's *t*-test, and * and ** indicate significance at the 0.05 and 0.01 levels of confidence, respectively.

encoded in the nucleus, showed no change during SuCMoV infection.

The impact of viral infection on PSI has been poorly investigated. PsaH and ferredoxin NADP+ oxidoreductase (FNR) showed a down-regulation at all stages of viral infection. PsaH is a peripheral protein involved in state transition, whereas FNR is one of rate-limiting steps in the photosynthetic electron transport. Plants deficient in state transitions or FNR activity were found to have chloroplast redox alteration, reduced photosynthesis rate, lower levels of total chlorophyll, and increased susceptibility to photooxidative damage under growth-light conditions [52,53]; these responses are similar to SuCMoV infection. FNR catalyzed the electron transfer from two molecules of ferredoxin to one of $NADP^+$ [54]. Interestingly, we detected a NADPH increase associated with the drop in *fnr* expression, suggesting that alternative pathways of NADPH production, such as oxidative pentose phosphate pathway (OPPP) and NADP-malic enzyme (NADP-ME), which have been related to viral infection, could be involved [55,56]. Furthermore, we observed pyridine nucleotide content increases without redox changes during sunflower–SuCMoV interaction. The pyridine nucleotides do not function as redox buffers themselves, but regulate the redox state of both electron transport carriers of chloroplasts and mitochondria and redox metabolites like ascorbate, glutathione and tioredoxin reduction [57]. Studies of mutants provide evidence that changes in NAD(P) content can alter photosynthesis and plant stress responses [58], and suggest that NAD(P) content could be a powerful modulator of metabolic integration [58].

Based on previous and the present results, we suggest a kinetic mechanistic model to explain chlorotic symptom development induced during sunflower–SuCMoV compatible interaction. SuCMoV inoculated in the first pair of leaves induced only one superoxide radical generation peak at 6 h post inoculation (hpi) in the second pair of leaves, which is followed by an increase in CAT (24 hpi) and SOD (48 hpi) activity [12]. SuCMoV reached the second pair of leaves at 4 dpi and induced sugar increase, photoinhibition, and increases in antioxidant enzyme activities, without any chlorotic effect. These redox related processes increased with chlorotic symptom appearance at 7 dpi (ES) and were even more marked at 12 dpi (LS), and it can be modulated by sugars [4]. Chlorotic symptom appearance is also accompanied by significant changes in major redox-related metabolites, such as decrease in apoplastic superoxide production and increase in: hydrogen peroxide, reduced glutathione and pyridine nucleotides. A shift in the pattern expression of genes related to cellular redox state, such as key genes related to antioxidant enzymes, photosynthesis and respiration was also observed. Hence, we suggest that

SuCMoV infection induces progressive changes in determinants of redox homeostasis that could be associated with chlorotic symptom development.

## Acknowledgments

This work was supported by grants from Consejo Nacional de Investigaciones Científicas y Técnicas (PIP-CONICET 6321), Agencia Nacional de Promoción Científica y Tecnológica (PICT 25982, PICT 2008 0067). MR and HRL are fellows of CONICET. We thank German Robert for technical assistance.

## Appendix A. Supplementary data

Supplementary data associated with this article can be found, in the online version, at http://dx.doi.org/10.1016/j.plantsci.2012.08.008.

## References

[1] S. Lenardon, F. Giolitti, A. León, M. Bazzalo, M. Grondona, Effect of *Sunflower chlorotic mottle virus* infection on sunflower yield parameters, HELIA 24 (2001) 55–66.
[2] A. Maule, V. Leh, C. Lederer, The dialogue between viruses and hosts in compatible interactions, Curr. Opin. Plant Biol. 5 (2002) 279–284.
[3] S. Whitham, C. Yang, M. Goodin, Global impact: elucidating plant responses to viral infection, Mol. Plant Microbe Interact. 19 (2006) 1207–1215.
[4] M. Rodríguez, E. Taleisnik, S. Lenardon, R. Lascano, Are *Sunflower chlorotic mottle virus* infection symptoms modulated by early increases in leaf sugar concentration? J. Plant Physiol. 167 (2010) 1137–1144.
[5] D. Bilgin, J. Zavala, J. Zhu, S. Clough, D. Ort, E. DeLucia, Biotic stress globally downregulates photosynthesis genes, Plant Cell Environ. 33 (2010) 1597–1613.
[6] L. Nooden, Introduction, in: L. Nooden (Ed.), Plant Cell Death Processes, Elsevier, Amsterdam, 2004, pp. 1–18.
[7] H. Kyseláková, J. Prokopová, J. Nauš, O. Novák, M. Navrátil, D. Šafářová, M. Špundová, P. Ilík, Photosynthetic alterations of pea leaves infected systemically by *Pea Enation Mosaic Virus*: a coordinated decrease in efficiencies of $CO_2$ assimilation and photosystem II photochemistry, Plant Physiol. Biochem. 49 (2011) 1279–1289.
[8] K. Asada, The water–water cycle in chloroplasts: scavenging of active oxygens and dissipation of excess photons, Annu. Rev. Plant Physiol. Plant Mol. Biol. 50 (1999) 601–639.
[9] L. del Río, G. Pastori, J. Palma, L. Sandalio, F. Sevilla, F. Corpas, A. Jiménez, E. López-Huertas, J. Hernández, The activated oxygen role of peroxisomes in senescence, Plant Physiol. 116 (1998) 1195–1200.
[10] M. Sagi, R. Fluhr, Superoxide production by plant homologues of the $gp91^{phox}$ NADPH oxidase. Modulation of activity by calcium and by *Tobacco Mosaic Virus* infection, Plant Physiol. 126 (2001) 1281–1290.
[11] C. Lamb, R. Dixon, The oxidative burst in plant disease resistance, Annu. Rev. Plant Physiol. Plant Mol. Biol. 48 (1997) 251–275.
[12] M.C. Arias, C. Luna, M. Rodriguez, S. Lenardon, E. Taleisnik, *Sunflower chlorotic mottle virus* in compatible interactions with sunflower: ROS generation and antioxidant response, Eur. J. Plant Pathol. 113 (2005) 223–232.
[13] M. Riedle-Bauer, Role of reactive oxygen species and antioxidant enzymes in systemic virus infections of Plants, J. Phytopatol. 148 (2000) 297–302.
[14] S. Clarke, P. Guy, D. Burritt, P. Jameson, Changes in the activities of antioxidant enzymes in response to virus infection and hormone treatment, Physiol. Plantarum 114 (2002) 157–164.
[15] R. Mittler, S. Vanderauwerab, M. Gollerya, F. Van Breusegem, Reactive oxygen gene network of plants, Trends Plant Sci. 9 (2004) 490–498.
[16] I. Gadjev, S. Vanderauwera, T. Gechev, C. Laloi, I. Minkov, V. Shulaev, K. Apel, D. Inze, R. Mittler, F. Van Breusegem, Transcriptomic footprints disclose specificity of reactive oxygen species signaling in Arabidopsis, Plant Physiol. 141 (2006) 436–445.
[17] G. Potters, N. Horemans, M. Jansen, The cellular redox state in plant stress biology – a charging concept, Plant Physiol. Biochem. 48 (2010) 292–300.
[18] C. Foyer, G. Noctor, Oxidant and antioxidant signaling in plants: a re-evaluation of the concept of oxidative stress in a physiological context, Plant Cell Environ. 28 (2005) 1056–1071.
[19] C. Foyer, G. Noctor, Redox homeostis and antioxidant signaling: a metabolic interface between stress perception and physiological responses, Plant Cell 17 (2005) 1866–1875.
[20] C. Foyer, G. Noctor, Redox regulation in photosynthetic organisms: signaling, acclimation, and practical implications, Antioxid. Redox Signal. 11 (2009) 861–905.
[21] S. Spoel, G. Loake, Redox-based protein modifications: the missing link in plant immune signaling, Curr. Opin. Plant Biol. 14 (2011) 358–364.
[22] G. Noctor, G. Queval, A. Mhamdi, S. Chaouch, C. Foyer, Glutathione The Arabidopsis Book, vol. 9, The American Society of Plant Biologists, USA, 2011, p. 0142.
[23] N. Bejerman, F. Giolitti, S. de Breuil, S. Lenardon, Molecular characterization of *Sunflower chlorotic mottle virus*: a member of a distinct species in the genus *Potyvirus*, Arch. Virol. 155 (2010) 1331–1335.
[24] A. Schneiter, J. Miller, Description of sunflower growth stages, Crop Sci. 21 (1981) 901–903.
[25] B. Hoel, K. Solhaug, Effect of irradiance on chlorophyll estimation with the Minolta SPAD-502 leaf chlorophyll meter, Ann. Bot. (Lond.) 82 (1998) 389–392.
[26] T. Candresse, M. Lanneau, F. Revers, S. Kofalvi, G. Macquaire, PCR-based techniques for the detection of plant viruses and viroids, Acta Horticult. (ISHS) 530 (2000) 61–67.
[27] G. Guilbault, P. Brignac, M. Juneau, New substrates for the fluorometric determination of oxidative enzymes, Anal. Chem. 40 (1968) 1256–1263.
[28] J. Anderson, B. Chevone, J. Hess, Seasonal variation in the antioxidant system of eastern white pine needles: evidence for thermal dependence, Plant Physiol. 98 (1992) 501–508.
[29] K. Gillespie, E. Ainsworth, Measurement of reduced, oxidized and total ascorbate content in plants, Nat. Protoc. 2 (2007) 871–874.
[30] G. Queval, G. Noctor, A plate-reader method for the measurement of NAD, NADP, glutathione and ascorbate in tissue extracts. Application to redox profiling during Arabidopsis rosette development, Anal. Biochem. 363 (2007) 58–69.
[31] M. Bradford, A rapid and sensitive method for the quantitation of microgram quantities of proteins utilizing the principle of protein-dye binding, Anal. Biochem. 72 (1976) 248–254.
[32] K. Livak, T. Schmittgen, Analysis of relative gene expression data using real-time quantitative PCR and the $2^{-\Delta\Delta ct}$ method, Methods 25 (2001) 402–408.
[33] M. Babu, J. Griffiths, T.-S. Huang, A. Wang, Altered gene expression changes in Arabidopsis leaf tissues and protoplasts in response to *Plum pox virus* infection, BMC Genomics 9 (2008) 325–346.
[34] R. Edwards, J.W. Blount, R.A. Dixon, Glutathione and elicitation of the phytoalexin response in legume cell culture, Planta 184 (1991) 403–409.
[35] M.J. May, K.E. Hammond-Kosack, J.D. Jones, Involvement of reactive oxygen species, glutathione metabolism and lipid peroxidation in the Cf-gene-dependent defence response of tomato cotyledons induced by race specific elicitors of *Cladosporium fulvum*, Plant Physiol. 110 (1996) 1367–1379.
[36] B. Karpinska, G. Wingsle, S. Karpinski, Antagonistic effects of hydrogen peroxide and glutathione on acclimation to excess excitation energy in Arabidopsis, IUBMB Life 50 (2000) 21–26.
[37] E. Hideg, C. Barta, T. Kalai, M. Vass, K. Hideg, K. Asada, Detection of singlet oxygen and superoxide with fluorescence sensors in leaves under stress by photoinhibition or UV radiation, Plant Cell Physiol. 43 (2002) 1154–1164.
[38] S. Herbette, C. Lennea, D. Tourvieille de labrouhe, J. Drevetc, P. Roeckel-Drevet, Transcripts of sunflower antioxidant scavengers of the SOD and GPX families accumulate differentially in response to downy mildew infection, phytohormones, reactive oxygen species, nitric oxide, protein kinase and phosphatase inhibitors, Physiol. Plant 119 (2003) 418–428.
[39] R. Mittler, E. Herr, B. Orvar, W. van Camp, H. Willekens, D. Inze, B. Ellis, Transgenic tobacco plants with reduced capability to detoxify reactive oxygen intermediates are hyper-responsive to pathogen infection, Proc. Natl. Acad. Sci. U.S.A. 96 (1999) 14165–14170.
[40] K. Burhenne, P. Gregersen, Up-regulation of the ascorbate-dependent antioxidative system in barley leaves during powdery mildew infection, Mol. Plant Pathol. 1 (2000) 303–314.
[41] S. Karpinski, C. Escobar, B. Karpinska, G. Creissen, P. Mullineaux, Photosynthetic electron transport regulates the expression of cytosolic ascorbate peroxidase genes in Arabidopsis during excess light stress, Plant Cell 9 (1997) 627–640.
[42] S. Karpinski, H. Reynolds, B. Karpinska, G. Wingsle, G. Creissen, P. Mullineaux, Systemic signalling and acclimation in response to excess excitation energy in Arabidopsis, Science 284 (1999) 654–657.
[43] S. Davletova, L. Rizhsky, H. Liang, Z. Shengqiang, D. Oliver, J. Coutu, V. Shulaev, K. Schlauch, R. Mittler, Cytosolic ascorbate peroxidase 1 is a central component of the reactive oxygen gene network of Arabidopsis, Plant Cell 17 (2005) 268–281.
[44] S. Dorey, F. Baillieul, P. Saindrenan, B. Fritig, S. Kauffmann, Tobacco class I and II catalases are differentially expressed during elicitor-induced hypersensitive cell death and localized acquired resistance, Mol. Plant Microbe Interact. 11 (1998) 1102–1109.
[45] S. Volk, J. Feierabend, Photoinactivation of catalase at low temperature and its relevance to photosynthetic and peroxide metabolism in leaves, Plant Cell Environ. 12 (1989) 701–712.
[46] S. Chivasa, A. Murphy, M. Naylor, J. Carr, Salicylic acid interferes with *Tobacco mosaic virus* replication via a novel salicylhydroxamic acid-sensitive mechanism, Plant Cell 9 (1997) 547–557.
[47] D. Maxwell, Y. Wang, L. McIntosh, The alternative oxidase lowers mitochondrial reactive oxygen production in plant cells, Proc. Natl. Acad. Sci. U.S.A. 96 (1999) 8271–8276.
[48] S. Berger, A. Sinha, T. Roitsch, Plant physiology meets phytopathology: plant primary metabolism and plant–pathogen interactions, J. Exp. Bot. 58 (2007) 4019–4026.
[49] K. Lehto, M. Tikkanen, J.-B. Hiriart, V. Paakkarinen, E.-M. Aro, Depletion of the photosystem II core complex in mature tobacco leaves infected by the *Flavum* strain of *Tobacco mosaic virus*, Mol. Plant Microbe Interact. 16 (2003) 1135–1144.

[50] K. Tiller, G. Link, Phosphorylation and dephosphorylation affect functional characteristics of chloroplast and etioplast transcription systems from mustard (*Sinapis alba* L.), EMBO J. 12 (1993) 1745–1753.
[51] J. Rahoutei, I. García-Luque, M. Barón, Inhibition of photosynthesis by viral infection: effect on PSII structure and function, Physiol. Plant 110 (2000) 286–292.
[52] C. Lunde, P. Jensen, L. Rosgaard, A. Haldrup, M. Gilpin, H. Scheller, Plants impaired in state transitions can to a large degree compensate for their defect, Plant Cell Physiol. 44 (2003) 44–54.
[53] J. Palatnik, E. Allen, X. Wu, C. Schommer, R. Schwab, J. Carrington, D. Weigel, Control of leaf morphogenesis by microRNAs, Nature 425 (2003) 257–263.
[54] R. Rodriguez, A. Lodeyro, H. Poli, M. Zurbriggen, M. Peisker, J. Palatnik, V. Tognetti, H. Tschiersch, M. Hajirezaei, E. Valle, N. Carrillo, Transgenic tobacco plants overexpressing chloroplastic ferredoxin-NADP(H) reductase display normal rates of photosynthesis and increased tolerance to oxidative stress, Plant Physiol. 143 (2007) 639–649.
[55] P. Díaz-Vivancos, M. Clemente-Moreno, M. Rubio, E. Olmos, J. García, P. Martínez-Gómez, J. Hernández, Alteration in the chloroplastic metabolism leads to ROS accumulation in pea plants in response to plum pox virus, J. Exp. Bot. 59 (2008) 2147–2160.
[56] V. Doubnerová, K. Müller, N. Čeřovská, H. Synková, P. Spoustová, H. Ryšlavá, Effect of potato virus Y on the NADP-Malic enzyme from *Nicotiana tabacum* L.: mRNA, expressed protein and activity, Int. J. Mol. Sci. 10 (2009) 3583–3598.
[57] G. Noctor, G. Queval, B. Gakiere, NAD(P) synthesis and pyridine nucleotide cycling in plants and their potential importance in stress conditions, J. Exp. Bot. 57 (2006) 1603–1620.
[58] C. Dutilleul, C. Lelarge, J. Prioul, R. De Paepe, C. Foyer, G. Noctor, Mitochondria-driven changes in leaf NAD status exert a crucial influence on the control of nitrate assimilation and the integration of carbon and nitrogen metabolism, Plant Physiol. 139 (2005) 64–78.